

## **COUPLING ERROR MODEL OF 3-DOF-COMPLIANT STAGE BASED ON PARALLELOGRAM MECHANISM**

**Huaibo Qiang<sup>1)</sup>, Hongxi Wang<sup>1)</sup>, Qiang Huang<sup>2)</sup>**

1) *Xi'an Technological University, School of Mechatronic Engineering, Xi'an 710021, China*  
(✉ [qianghuaibo@xatu.edu.cn](mailto:qianghuaibo@xatu.edu.cn))

2) *Northwest Institute of Mechanical & Electrical Engineering, Xianyang 712099, China*

### **Abstract**

Compliant mechanisms are the state-of-the-art in precision Compliant Parallelogram Stage (CPS) due to their many beneficial features. However, the translational motion of CPS is accompanied by parasitic displacement and coupling error in these mechanisms. In this paper, the parasitic displacements are analysed by firstly applying the pseudo-rigid-body theory to One-Degree of Freedom (1-DoF) CPS. Then the theoretical model of the Coupling Error Transfer Matrix (CETM) is presented on a Three-Degree of Freedom (3-DoF) serial CPS. Moreover, the general forms of CETM are developed for the various configurations of 3-DoF-compliant mechanisms. In addition, the coupling error model is validated through experiment on a 1-DoF CPS. Meanwhile, the analytical results are validated with Finite Element Analysis (FEA) by comparing the parasitic displacements on each coordination axial direction. Compared with the analysis results between theoretical calculation and the FEA method, the maximum difference of the parasitic displacement is about  $0.18 \mu\text{m}$  and the relative error of about 6.22%. This result offers effective ways to calculate and compensate for the coupling errors and serves to facilitate further work regarding the precision analysis of compliant mechanisms.

Keywords: Compliant Parallelogram stage, Parasitic displacement, Coupling error, Transfer matrix.

### **1. Introduction**

Compliant mechanisms constitute a crucial branch of modern mechanics which applies elastic deformation of flexible materials to transmit motion and power [1]. Compared with traditional rigid mechanisms, compliant mechanisms have many advantages, such as zero backlash, lubrication-free, no friction and wear, smooth and continuous motion, compact structures and displacement resolution up to 1 nm [2]. Therefore, they have been extensively employed in high-precision applications such as surgical tools, micro-grippers, micro/nano manipulators and even precise measurement mechanisms.

Flexure hinges [3], parallel springs [4] and flexible diaphragms [5] are widely used in measurement mechanisms and micro-positioning systems. For example, the compliant parallelogram plates are employed in both the Renishaw SP80 probe and Klingelnberg K3D probe [6] that are serve

as the translational displacement units. Over the last two decades, compliant mechanisms have assumed increasingly critical roles in precise transmission fields. Research in the field of compliant mechanisms is rapidly increasing due to extensive applications of Micro-Electro-Mechanical Systems technology.

However, the accompanying parasitic motion and coupling error can adversely affect the displacement accuracy and working characteristics during the operation of a CPS [7]. Therefore, it is essential to analyse the reason for parasitic displacement and coupling errors in the CPS. These efforts could establish a good foundation for taking reasonable measures to reduce the adverse impact of coupling errors on CPSs. So far, some solutions have been proposed to increase the motion precision of compliant mechanisms. For instance, the precise movements of displacement of flexure hinges were negatively affected by stiffness reduction in bearing directions [8]. Meanwhile, the manufacturing tolerances of flexible beams can adversely affect the bearing direction stiffness and error motions. The theoretical parasitic rotational angle of the compliant module was analysed with respect to the axial deformations of the beams [9].

Moreover, analytical methods have been proposed that are based on the mathematical description of compliant mechanisms. The theoretical models of the mechanisms' natural frequency were established by using the Lagrange equation [10]. The geometric compatibility equations were combined to describe the coupling effects among kinematic chains [11]. Addressing the issue of parasitic rotation in compliant mechanisms between the fixed base and motion parts, a non-under-constrained compliant module was developed to constrain the parasitic rotation and lost motion [12]. Furthermore, an analytical method was formulated for parasitic rotation and displacement calculations of a CPS [13]. The actuator can obtain continuous linear motion by the parasitic motion of the asymmetrical-trapezoid-compliant mechanisms [14].

On the other hand, the several compliant parallelogram units can be assembled in various arrangements. Double parallelogram guide mechanisms were added at the output ends of the bridge-type mechanisms to minimize the parasitic movements of the XY mechanism [15]. The motion errors in the bearing direction can be reduced by arranging two parallelogram-compliant modules in a nested parallel arrangement [16]. The existence of complex non-minimum phase zeros was presented in two double parallelogram mechanisms [17]. Additionally, the coupling motion of compliant parallelogram modules would be partially eliminated because the topology structure was kineto-statically decoupled [18].

Based on previous studies, the current research on parasitic displacement and error compensation has been mostly limited to single-degree of freedom mechanisms. Meanwhile, these studies were largely focused on the theoretical model of flexible elements and analysis of the relationship between load and stiffness. Yet, comparatively little research has been done on the coupling error of multi-degrees of freedom CPSs.

This paper presents a novel theoretical model of parasitic displacement and coupling error which are the research highlights on the CPS. A series of 3-DoF CPS is proposed in Section 2. The CETM of the 3-DoF CPS is established and the coupling-error relationships are described under different topological structures in Section 3. The correctness of this theoretical model is verified by the experimental investigation and FEA simulation. Finally, conclusions are given in Section 5.

## **2. Principle of the 3-DoF translational stage**

The common compliant structural forms include flexure hinges, flexible beams [2], parallel springs [4] and flexible diaphragms [6]. In the field of MEMS systems, flexible elements are used as translational or guiding mechanisms with the displacement reaching the micro-meter

level. They are often composed of a single parallelogram unit or several parallelogram units to meet high-precision and large-stroke transmission requirements. Figure 1 shows the schematic diagram of a serial model of the 3-DoF translational mechanism. The centre of the measuring ball is defined as the coordinate origin  $O$  while the directions of the three orthogonal axes are the  $x$ -axis,  $y$ -axis and  $z$ -axis respectively. The reverse direction of the stylus feed is defined as the  $z$ -axis. The complex spatial movements can be decomposed and guided using the translational motion on each axial compliant guidance unit.

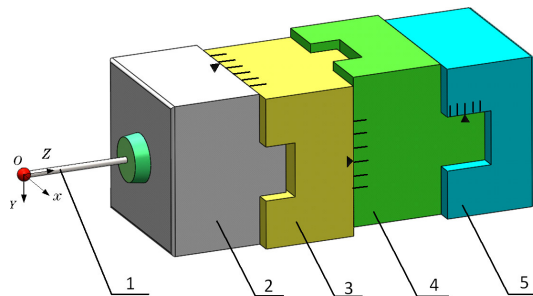


Fig. 1. The series model of the 3-DoF translational stage, 1) stylus, 2) the  $x$ -axial translational unit, 3) the  $y$ -axial translational unit, 4) the  $z$ -axial translational unit, 5) the fixed base.

The displacements of each translational unit are measured through the internal sensors of the compliant mechanisms. Hence, the geometric information is calculated according to the measurement point information such as the size and shape of the measured objects. The input driving force is transmitted to the compliant guidance mechanism by the stylus when the external measuring stylus contacts the measured object. The general working stroke range of a precision 3D scanning probe is  $\pm 1\text{--}2.5$  mm, the measurement driving force is  $\pm 0.1\text{--}0.5$  N and the resolution can reach the level of  $0.01\text{--}0.02$   $\mu\text{m}$  [19].

The sliding or rolling guide pairs were rarely used in the guiding mechanism of precision translational motion because these guide pairs are not only dependent on the relative contact surface to provide certain preloading force and reasonable lubrication conditions but also on some reset devices to ensure the smoothness and continuity of guiding movement.

However, for these pairs it is difficult to meet the performance requirements of the guiding mechanism in precise measurement or positioning systems. Ideally, the transmission process of the translational mechanism is approach its being frictionless, gapless and compact. These requirements are well adapted to use the Compliant Parallelogram Stage to construct miniaturized or even miniaturized translational motion mechanisms. Hence, it is suitable as a CPS for precise positioning or micro-measurement systems [20].

### 3. Coupling error of CPS

Parasitic displacement is an accompanying displacement which is generated in the vertical direction of the main motion direction in mechanisms. The coupling effect among different motion units can have a significant influence on the motion accuracy and performance of an integral CPS.

For example, the 3-DoF-compliant translational units of a precision scanning probe can be combined in serial, parallel or serial-parallel hybrid structure. The coupling errors and parasitic displacements are presented in different forms according to these various topological structures. Therefore, it is necessary to analyse the principle of coupling errors in different configurations of CPS, and some reasonable measures can be taken to reduce the negative impact of coupling errors on CPS.

### 3.1. Parasitic displacement of 1-DoF CPS

Figure 2 shows the pseudo-rigid-body model of the 1-DoF Compliant Parallelogram Stage. Therein the undeformed initial situation is represented by solid lines and the deformed situation is represented by dashed lines. According to the pseudo-rigid body theory [21, 22], the flexible guide plate is equivalent to a rigid element and the flexure hinges at both ends of each guide plate are equivalent to the ideal rotational pairs. This CPS is fixed to the base and loaded with the input driving force  $F$  on the end of the stylus. The pseudo-rigid-body angle  $\theta$  of the compliant guide plates is caused by elastic deformation of the flexure hinges. The parasitic displacement  $\delta$  in the  $y$ -axial direction is caused by the translational displacement  $\Delta x$  in the  $x$ -axial direction which can be represented as:

$$\delta = l - \sqrt{l^2 - \Delta x^2}, \tag{1}$$

where  $l$  is the length of the compliant guide plates. The dimensionless expression  $\lambda$  is introduced which is defined as  $\lambda = \Delta x/l$ . The parameter  $\eta$  can be expressed as  $\eta = \delta/l$  in the coupling error coefficient of the CPS, then (1) can be written as:

$$\eta = 1 - \sqrt{1 - \lambda^2}. \tag{2}$$

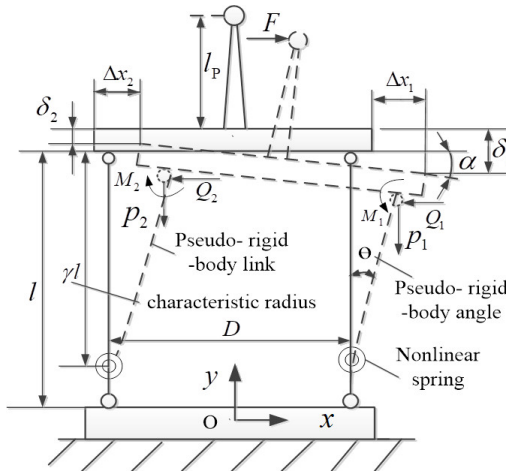


Fig. 2. Pseudo-rigid-body model of 1-DOF CPS.

The translational displacement  $\Delta x$  is along the main motion direction of the input driving force  $F$  while the direction vector of parasitic displacement  $\delta$  is perpendicular to the translational displacement  $\Delta x$ . Furthermore, the parasitic displacement  $\delta$  is affected by the material and some structural parameters of the two compliant plates. Generally, there is  $\Delta x \leq l$  in the precision translational guidance and micro-positioning mechanisms.

If the polynomial  $\sqrt{1 - \lambda^2}$  is expanded by using the Taylor expansion:

$$\sqrt{1 - \lambda^2} = 1 - \frac{\lambda^2}{2} + \dots + R_n(\lambda) \approx 1 - \frac{\lambda^2}{2}. \tag{3}$$

If the formula (3) is substituted into (2), the error coupling coefficient is obtained as:

$$\eta = \frac{1}{2}\lambda^2 = \frac{1}{2}\left(\frac{\Delta x}{l}\right)^2 \approx \frac{1}{2}\theta^2. \tag{4}$$

In (4), the driving force  $F$  is the combined action on the compliant guide plates on both sides of the parallelogram mechanism. The value of the pseudo-rigid-body angle  $\theta$  is the ratio of the translational displacement  $\Delta x$  to the length  $l$  of compliant plates. According to the equation in the references [23], the parasitic displacement  $\delta$  can be expressed as:

$$\delta = l - \gamma l \sin \theta = l(1 - \gamma \sin \theta). \quad (5)$$

Here,  $\gamma$  is the characteristic radius factor. A simple rule-of-thumb for  $\gamma$  in rough calculations is  $\gamma = 0.85$ . Once  $\gamma$  is determined, the deflection path may be parameterized in terms of  $\theta$ , the pseudo-rigid-body angle. For this reason, the pseudo-rigid-body angle  $\theta$  will increase accordingly when the CPS is improved to achieve a large stroke, but the parasitic displacement  $\delta$  will be decreased conversely. As a result, the larger value of the pseudo-rigid-body angle  $\theta$  would not affect the estimation of parasitic displacements in compliant guiding mechanisms.

The parasitic rotation of the guiding plate occurs when the axial deformations of the two compliant plates are considered. With a right horizontal force  $F$  acting on the translational plate, the left compliant plate will be extended by an axial force  $P_2$  and the right compliant plate will be compressed by another axial force  $P_1$ . Parasitic displacement  $\delta_1$  and  $\delta_2$  are the axial deformations of the right and the left compliant plates respectively. The parameter  $\alpha$  is the parasitic angle of the guiding plate and  $D$  is the distance between two compliant plates. As the symmetry of this structure is about the  $y$ -axis, the force  $F$  and moment  $M$  acting on two compliant plates are almost the same. From the geometry relations and balance of forces and moments in Fig. 2, the following equations can be presented as:

$$\begin{cases} M_1 + M_2 - Fl_p \cos \alpha + (Q_1 + Q_2) \frac{D}{2} \sin \alpha + (P_1 + P_2) \frac{D}{2} \cos \alpha = 0 \\ D \sin \alpha + \delta_2 = \delta_1 \\ \Delta x_1 = \Delta x_2 = -\frac{Q_1 l^3}{3EI} = -\frac{Q_2 l^3}{3EI} \\ F = P_1 + P_2 \end{cases}, \quad (6)$$

where  $\alpha$  is very small angle in small deformation. Then  $\sin \alpha \approx \alpha$  and  $\cos \alpha \approx 1$ , so the parasitic angle of this CPS can be calculated as below:

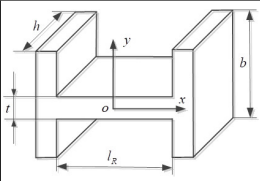
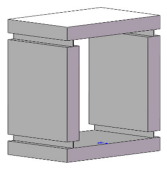
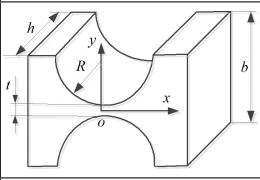
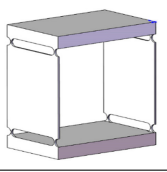
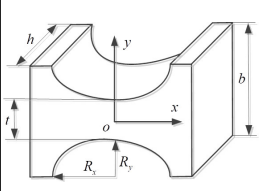
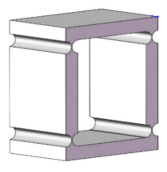
$$\alpha = \frac{F(l + l_p)^2}{E(hlD^2 + 4I)}. \quad (7)$$

This type of a 1-DoF CPS is applied in precision mechanisms such as scanning probes or precise positioning mechanisms. The range of displacement is several milli-meters and the driving force  $F$  is relatively smaller. It is commonly as little as 0.5 N approximately. When the length of the stylus is  $l_p = 28$  mm, the values of the other parameters are shown in following Table 3. The calculated value of parasitic angle  $\alpha$  is  $2.08 \times 10^{-7}^\circ$ . Therefore, the parasitic motion of the guiding plate can be negligible.

The different flexure hinges are adopted in various compliant mechanisms, such as the rectangular flexure hinge, right-circular flexure hinge and elliptical flexure hinges. The similar structure of a 1-DoF CPS is built with different flexure elements. The distinct stiffness of these flexure hinges and the stiffness of a 1-DoF CPS are listed in Table 1 respectively.

Parameter  $t$  is the minimum thickness which is an important index of stiffness performance in flexure hinges. The stiffness  $K_{\text{hinge}}$  of the flexure hinge increases with the increase of the minimum thickness  $t$ .

Table 1. Stiffness of three types of compliant stages with their corresponding flexure hinges.

Types	Structure of compliant units	Formula for stiffness
Rectangular flexure hinge		$K_{\text{hinge}} = \frac{Eht^3}{12l_R}$
CPS built with rectangular flexure hinges		$K_{\text{stage}} = \frac{Eht^3}{3l_R l^2}$
Right-circular flexure hinges		$K_{\text{hinge}} = \frac{Eh^3}{24 \left( \frac{t+2R}{\sqrt{t(t+4R)}} \arctan \left( \frac{t+2R}{\sqrt{t(t+4R)}} \right) - \frac{\pi}{4} \right)}$
CPS built with right-circular flexure hinges		$K_{\text{stage}} = \frac{Eh^3}{6l^2 \left( \frac{t+2R}{\sqrt{t(t+4R)}} \arctan \left( \frac{t+2R}{\sqrt{t(t+4R)}} \right) - \frac{\pi}{4} \right)}$
Elliptical flexure hinges		$K_{\text{hinge}} = \frac{Eha_y^3}{12a_x} \left[ \frac{12(a_y/t)^4(2a_y/t+1)}{(4a_y/t+1)^{1/2}} \arctan \sqrt{4a_y/t+1} + \frac{2(a_y/t)^3 \left( \frac{16a_y^2}{t} + 4a_y/t+1 \right)}{(4a_y/t+1)^2 + 2(a_y/t+1)} \right]^{-1}$
CPS built with elliptical flexure hinges		$K_{\text{stage}} = \frac{Eha_y^3}{3a_x l^2} \left[ \frac{12(a_y/t)^4(2a_y/t+1)}{(4a_y/t+1)^{1/2}} \arctan \sqrt{4a_y/t+1} + \frac{2(a_y/t)^3 \left( \frac{16a_y^2}{t} + 4a_y/t+1 \right)}{(4a_y/t+1)^2 + 2(a_y/t+1)} \right]^{-1}$

Based on the theory of the Flexible Beam Bending principle, the swing angle of the single-sided compliant guide plates is  $\theta = Fl^2/4EI\theta = Fl^2/4EI$ . The elastic modulus  $E$  should be corrected to the plane elastic modulus  $E'$  when the ratio of width  $b$  to thickness  $h$  is more than 10 times for the compliant guide plates, and the correction relationship is shown in (8):

$$E' = \frac{E}{1 - \mu^2}. \quad (8)$$

In the equation above, the parameter  $\mu$  is the Poisson's ratio for the flexible material of the compliant guiding plates. The parasitic displacement  $\delta$  of a 1-DoF on CPS can be expressed as:

$$\delta = \frac{F^2 l^5}{32(E'I)^2}, \quad (9)$$

where  $E'I$  is the bending stiffness and the section is a rectangle consisting of the compliant guide plates. The moment of inertia is  $I = lh^3/12$  when the bending deformation occurs in the compliant plates. Therefore, in such case, the expression of the parasitic displacement  $\delta$  is adapted as:

$$\delta = \frac{9F^2 l^5}{2E'^2 h^6}. \quad (10)$$

### 3.2. Coupling error of 3-DoF CPS

The higher the degree of freedom in compliant mechanisms, the more parasitic displacement and coupling error would exist in these mechanisms. Coupling errors are an important source of errors in compliant mechanisms such as precision probes or micro positioning systems. This research focuses on exploring the principles of coupling error in the compliant stage and establishing the *Coupling Error Transfer Matrix* (CETM). The aim is to develop the theoretical model for improving the motion accuracy and comprehensive performance of CPS. In this section, three units of a 1-DoF CPS were arranged in series to constitute a 3-DoF-compliant guiding mechanism in the probe, as shown in Fig. 3. The axial direction of the stylus is defined as the  $z$ -axis. Some insignificant factors were disregarded in this study, such as deformation of the stylus and radius errors of the measuring ball.

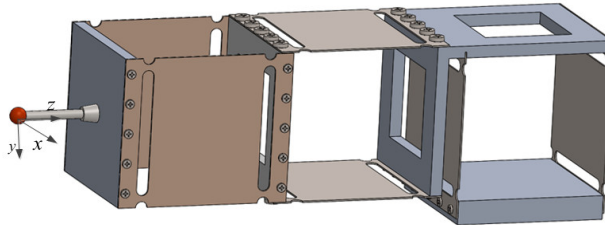


Fig. 3. Serial configuration of a 3-DoF CPS.

Assuming that the ideal translational output displacements are  $\Phi = (\Delta x, \Delta y, \Delta z)^T$  given by three sensor units that are fitted inside each compliant stage, it can be concluded that there are coupling errors in the compliant guidance mechanism along the three coordinate axes. The CETM of the 3-DoF-compliant parallelogram guidance mechanism is expressed as:

$$\Gamma = (\delta_{ij}). \quad (11)$$

In this equation,  $\delta_{ij}$  represents the coupling error of the compliant stage in the  $i$ -axial direction, which is caused by the motion of the compliant stage in the  $j$ -axial direction, where  $i, j = x, y, z$ . The actual output translational displacement of the 3-DoF-compliant translational mechanism can be defined as  $\Lambda = (x_p, y_p, z_p)^T$ :

$$\Lambda = \Phi + \Gamma, \quad (12)$$

$$\begin{bmatrix} x_p \\ y_p \\ z_p \end{bmatrix} = \begin{bmatrix} \Delta x \\ \Delta y \\ \Delta z \end{bmatrix} + \begin{bmatrix} \delta_{xx} & \delta_{xy} & \delta_{xz} \\ \delta_{yx} & \delta_{yy} & \delta_{yz} \\ \delta_{zx} & \delta_{zy} & \delta_{zz} \end{bmatrix} \begin{bmatrix} 1 \\ 1 \\ 1 \end{bmatrix} = \Phi + \delta_{ij}e^r, \quad (13)$$

where  $\delta_{xx}$ ,  $\delta_{yy}$ ,  $\delta_{zz}$  are the inherent characteristic errors of the internal sensors of the CPS. Assuming that the inessential influence of intrinsic characteristics of each sensor was ignored in the compliant mechanism, so that there is  $\delta_{xx} = \delta_{yy} = \delta_{zz} = 0$ , (13) can be written as:

$$\begin{bmatrix} x_p \\ y_p \\ z_p \end{bmatrix} = \begin{bmatrix} \Delta x \\ \Delta y \\ \Delta z \end{bmatrix} + \begin{bmatrix} 0 & \delta_{xy} & \delta_{xz} \\ \delta_{yx} & 0 & \delta_{yz} \\ \delta_{zx} & \delta_{zy} & 0 \end{bmatrix} \begin{bmatrix} 1 \\ 1 \\ 1 \end{bmatrix} = \Phi + \Gamma e^r. \quad (14)$$

Considering the configuration relationship of the 3-DoF-compliant guidance mechanism in Fig. 3, the three-axial translational displacement is measured respectively by each sensor which is installed inside each stage. It is due to the parasitic displacements of the y-axial and z-axial CPS present without those along the x-axis. The reading for the x-axial sensor only contains the translational displacement of the x-axial CPS, resulting in  $\delta_{xy} = 0$ ,  $\delta_{xz} = 0$ .

Meanwhile, the coupling impact of the z-axial CPS does not act on the y-axial CPS because the parasitic displacement of the z-axial CPS is presented along y-axis while the parasitic displacement of the x-axial CPS does not occur along the y-axial CPS, so  $\delta_{yx} = 0$ ,  $\delta_{yz} = 0$ .

For the same reason, the parasitic displacements of the x-axial and y-axial CPS are both present along the z-axis, thus the reading for the z-axial sensor not only comprises the translational displacement of the z-axial CPS, but also the parasitic displacements of the x-axial and y-axial CPS simultaneously. Therefore, the corresponding matrix elements should be considered as  $\delta_{zx} \neq 0$ ,  $\delta_{zy} \neq 0$ .

Therefore, the relationship expression can be obtained between the actual output translational displacement  $(x_p, y_p, z_p)^T$  and the measurement results  $(\Delta x, \Delta y, \Delta z)^T$  along with three axes of the compliant mechanism as follows:

$$\begin{cases} x_p = \Delta x \\ y_p = \Delta y + \delta_{yz} \\ z_p = \Delta z + \delta_{zx} + \delta_{zy} \end{cases}. \quad (15)$$

Then the CETMG of this compliant parallelogram mechanism can be expressed as:

$$\Gamma = \begin{bmatrix} 0 & 0 & 0 \\ 0 & 0 & \delta_{yz} \\ \delta_{zx} & \delta_{zy} & 0 \end{bmatrix}. \quad (16)$$

Based on the research conclusion of the parasitic displacement model of a 1-DoF CPS above, the stroke ratio is  $\lambda_i = \Delta i / l_i$  ( $i = x, y, z$ ). According to formulas (1) and (9), the coupling error on the z-axial compliant stage, which is caused by the motion of the x-axis directional CPS, can be calculated as:

$$\delta_{zx} = \left(1 - \sqrt{1 - \lambda_x^2}\right) l_x = \frac{F_x^2 l_x^5}{32(E'I)^2}. \quad (17)$$

For the same reason, the coupling error on the z-axial compliant stage caused by the motion of the y-axis directional compliant parallelogram stage can be determined as:

$$\delta_{zy} = \left(1 - \sqrt{1 - \lambda_y^2}\right) l_y = \frac{F_y^2 l_y^5}{32(E'I)^2}. \quad (18)$$



Similarly, the coupling error on the y-axial compliant stage caused by the motion of the z-axis directional compliant parallelogram stage can be described as:

$$\delta_{yz} = \left(1 - \sqrt{1 - \lambda_z^2}\right) l_z = \frac{F_z^2 l_z^5}{32(E'I)^2}. \quad (19)$$

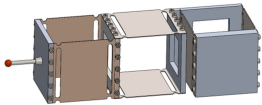
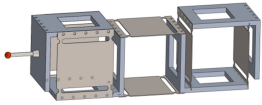
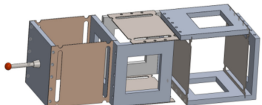
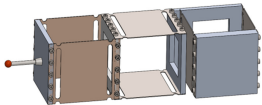
In the formula,  $F_x$ ,  $F_y$  and  $F_z$  are the components of the input driving force in the three coordinate axes respectively. The cross-sectional shape of the compliant guide plates is rectangular. Assuming that the characteristics of the compliant guide plates are consistent in terms of the same materials, structure and cross-sectional dimensions, the matrix of the CETM  $\Gamma$  can be then expressed as the following formula (20).

From (14), it can be observed that the elements of the CETM  $\Gamma$  would vary because of the different forms of the 3-DoF CPS. By substituting the results above into (12), the output translational displacement can be obtained which contains the coupling errors  $\Lambda = (x_p, y_p, z_p)$  for the 3-DoF CPS.

$$\Gamma = \frac{1}{64} \begin{bmatrix} 0 & 0 & 0 \\ 0 & 0 & \frac{F_z^2 l_z^5}{(E'I)^2} \\ \frac{F_x^2 l_x^5}{(E'I)^2} & \frac{F_y^2 l_y^5}{(E'I)^2} & 0 \end{bmatrix}. \quad (20)$$

Different topological configurations of CETM can be developed if the spatial position and connection form of several compliant mechanisms are altered in Fig. 3. The form of CETM is independent of the combination order of the 3-DoF CPS. Nevertheless, the form of CETM is related to the coordinate axial vectors of each compliant mechanism. The position of elements in the CETM will change only if some compliant mechanism rotates by  $\pm\pi/2$  phase angle about its own axis. The normal form of the CETM of the 3-DoF CPS is listed in Table 2.

Table 2. Forms of CETM according to the different configurations of the 3-DoF CPS.

Assembly scheme	Configuration of CPS	Form of CETM
$x \rightarrow y \rightarrow z$		$\begin{bmatrix} 0 & 0 & 0 \\ 0 & 0 & \delta_{yz} \\ \delta_{zx} & \delta_{zy} & 0 \end{bmatrix}$
$x$ -axial CPS rotates $\frac{\pi}{2} \rightarrow y \rightarrow z$		$\begin{bmatrix} 0 & 0 & 0 \\ \delta_{yx} & 0 & 0 \\ \delta_{zx} & \delta_{zy} & 0 \end{bmatrix}$
$x \rightarrow y$ -axial CPS rotates $\frac{\pi}{2} \rightarrow z$		$\begin{bmatrix} 0 & \delta_{xy} & 0 \\ 0 & 0 & 0 \\ \delta_{zx} & \delta_{zy} & 0 \end{bmatrix}$
$x \rightarrow y \rightarrow z$ -axial CPS rotates $\frac{\pi}{2}$		$\begin{bmatrix} 0 & 0 & \delta_{xz} \\ 0 & 0 & 0 \\ \delta_{zx} & \delta_{zy} & 0 \end{bmatrix}$

For multi-DoF CPS with parallel relationship, the connection and the coupling relationship should be analysed first, the CETM as in (14) can be established according to the combination form of the CPS.

For instance, as shown in Fig. 3, the CETM will remain the  $3 \times 3$  matrix, while the y-axial CPS is parallel to the x-axial CPS. Then the coupling impact of the y-axial CPM on the z-axial CPS is the same as that is the effect on the x-axial CPM, so  $\delta_{zy} = 0$  and  $\delta_{zx} = 0$ . Similarly, there are  $\delta_{zx} \neq 0$  and  $\delta_{zy} \neq 0$  when the x-axial CPM is parallel to the y-axial CPS in the 3-DoF CPS.

#### 4. FEM and experimental investigation

The prototype of the 1-DoF CPS was fabricated and evaluated with varying experimental parameters. Furthermore, the validation of analytical results of the coupling error model was provided by a FEA simulation in commercial ANSYS Workbench software.

##### 4.1. Analysis of 1-DoF CPS

The right-circular flexure hinge was constructed with the performance parameters and dimensions listed in Table 3. The compliant guide plates were fabricated with the wire-electrode cutting technique which offers a manufacturing tolerance of  $\pm 2 \mu\text{m}$ . The other components of the assembly, including the translational plates and fixed base, were fabricated by traditional machining.

Table 3. Parameters of the flexure hinge and compliant plate.

Parameter name	Symbol	Value	Unit
Elastic modulus of the flexure element	$E$	$1.95 \times 10^{11}$	GPa
Poisson's ratio of the flexure element	$\mu$	0.30	-
Length of the compliant plate	$l$	50.00	mm
Thickness of the compliant plate	$h$	0.30	mm
Radius of the flexure hinges	$R$	1.50	mm
Thickness of the compliant plate	$t$	1.00	mm
Distance between two compliant plates	$D$	50	mm

Stainless steels with Young's modulus of  $E = 195 \text{ GPa}$  was selected as the material for the compliant guide plates and aluminium alloy with Young's modulus of  $E = 73 \text{ GPa}$  was selected as the material of the translational plate and the fixed plate respectively. Besides the stylus, the whole size (length  $\times$  width  $\times$  height) of the 1-DoF compliant mechanism is  $50 \text{ mm} \times 50 \text{ mm} \times 55 \text{ mm}$ .

As shown in Fig. 4, the fixed constraints were applied above and below of the mounting base. Since the stiffness of the translational plates and the mounting base is much higher than that of the compliant guide plates, all of the translational plates and mounting base including the stylus were set to have the behaviour of utter stiffness.

The size for flexure hinges was set as 0.01 mm on the local element mesh. The input driving force was added matching the overall stiffness of the compliant mechanism so that the range of the force was 0–1 N and the step-size was 0.1 N.

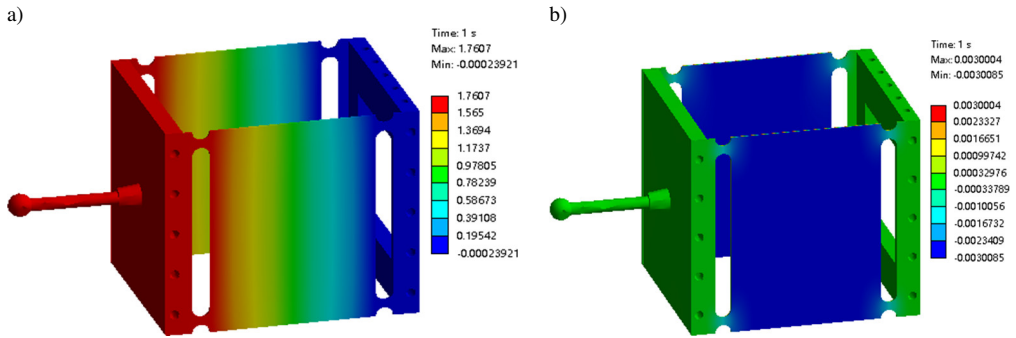


Fig. 4. Finite element results for the 1-DoF CPS (a) Translational displacements in  $x$ -axis, (b) Parasitic displacements in  $z$ -axis.

According to the FEA simulation, the maximum translational displacement in the  $x$ -axis was 1.7607 mm and the maximum parasitic displacement was 0.003 mm over the full travel range of the external driving force, respectively.

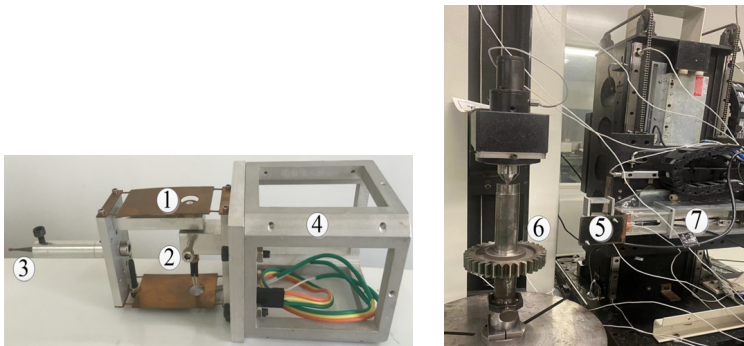


Fig. 5. Experimental setup and its components 1) CPS, 2) sensor, 3) stylus, 4) mounting base, 5) 1-DoF CPS, 6) tested object, 7) driving mechanism.

For the verification of the FEA results, an experimental setup was developed as shown in Fig. 5. The 1-DoF compliant guiding mechanism was installed on the CNC gear measurement device. The servo-driving unit of this experimental setup was adapted by application of a high-precision rolling screw-nut mechanism. Two-channel displacement information was identified effectively by LVDT differential displacement sensors.

Based on this experimental data, the theoretical curve, FEA results and the experimental curve of the translational displacement and parasitical displacement of the CPS were drawn as shown in Fig. 6.

According to Hook's law, the analytical method of determining the theoretical curve of translational displacement is calculated by using the formula as  $\Delta x = F_x / K_x$ , while the value of input force  $F_x$  increase on the  $x$ -axis from 0 ~ 1 N with the step-size of 0.5 N, then the theoretical curve is drawn using the formula above.

In the range of the input driving force, the maximum values of the translational displacement in theoretical calculation and experimental measurement were 1.7527 mm and 1.8013 mm, respectively, which constituted a relative error not exceeding 2.8% in the  $x$ -axis. The maximum values of parasitical displacement in theoretical calculation and experimental measurement were

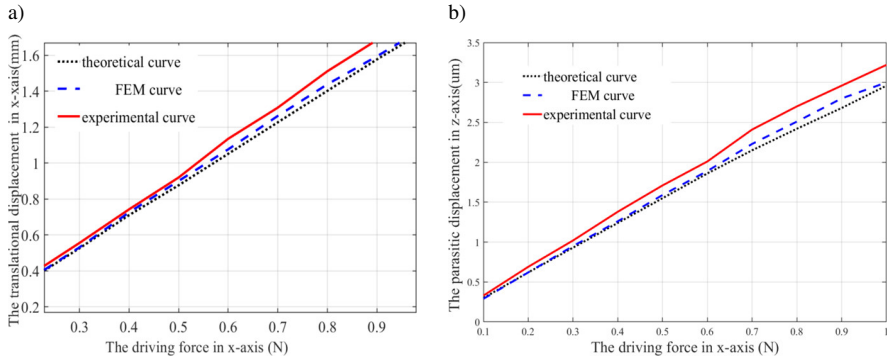


Fig. 6. Analytical and FEA results on 1-DoF CPS (a) Translational displacement in the  $x$ -axis, (b) Parasitical displacement in the  $z$ -axis.

0.0031 mm and 0.0033 mm respectively which constituted a relative error not exceeding 6.5% on the  $z$ -axis. On the other hand, the coupling errors occurring were shown in Fig. 6. over their full travel range in this compliant mechanism. This result verifies the accuracy and effectiveness of the coupling error theoretical model for the 1-DoF CPS.

It can be seen that the error result keeps increasing between the theoretical method and experiment data. The main reason is that this CETM is a relatively simplified error model where other factors are not considered, such as nonlinearity and vibration. However, those factors would produce errors in the result of the measurement with the increase of the driving force  $F$  during the experimental process.

To avoid these problems, some further attempts still need to be made in the future to improve the accuracy of the CETM, such as using lumped compliant units instead of distributed compliant units in a large deflection-compliant mechanism.

#### 4.2. FEA method for the 3-DOF CPS

To validate the coupling error theoretical model of the 3-DoF CPS, an FEA model was built in ANSYS Workbench with the FEA model setup as shown in Fig. 7. Stainless steel was selected as the material for the compliant guide plates and its performance parameters are detailed in Table 3. Both the translational plates and fixing base have a thickness of 5 mm and the material selected for them was aluminium alloy.

The compliant mechanisms were modelled with a size of 1 mm globally and refined in the areas of all the flexure hinges and the compliant plates by element sizes of 0.1 mm, as can be seen in Fig. 7. The shell elements were used to model the flexure hinges and compliant plates. The other physical properties and mesh conditions were selected in the same way as those presented in Section 4.1. The reference coordinate system was consistent with that shown in Fig. 3 and the fixed support constraints were provided on both sides of the end fixing plate. The three-axial external driving forces ( $F_x = 0.10$  N,  $F_y = 0.10$  N,  $F_z = 0.10$  N) were applied orthogonally along each coordinate axis at the root of the stylus.

Furthermore, the results for the deformation cloud map of this 3-DoF-compliant guidance mechanism were shown in Fig. 7. The displacements of the compliant translational plates were measured as well as the parasitic displacements which were tracked to evaluate the coupling errors according to (20). Similarly, the FEA methods were applied to all of the investigated compliant mechanisms.

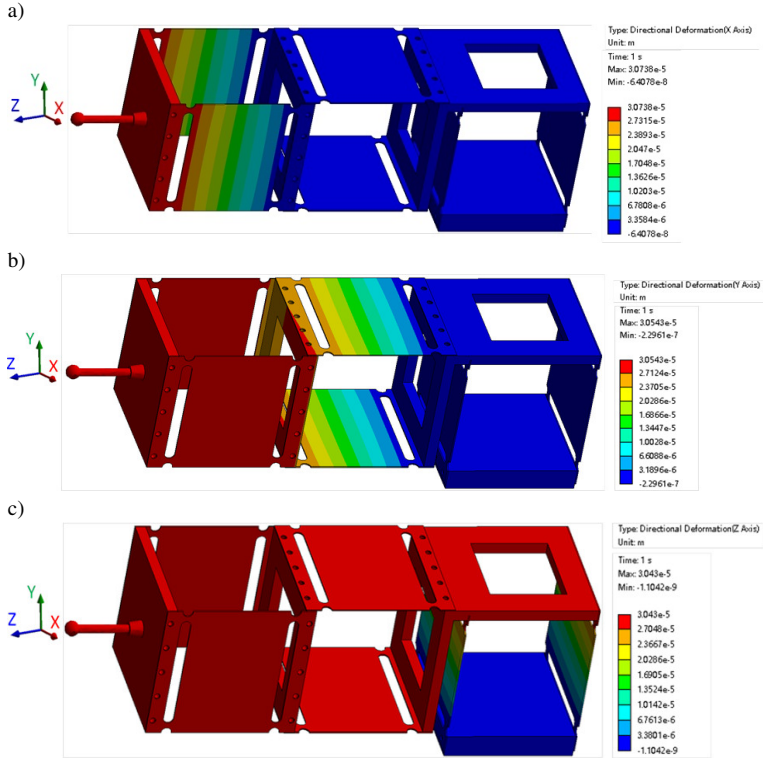


Fig. 7. FEA Model Setup and Results (a) the displacement results in the  $x$ -axis, (b) the displacement results in the  $y$ -axis, (c) the displacement results in the  $z$ -axis.

The difference is presented between the theoretical calculations and FEA maximum in Table 4 which shows the parasitic displacements in different coordinate axes as configurations in Fig. 7. The relative error of parasitic displacement is 3.75% in the  $z$ -axial direction. Moreover, the maximum value of coupling error is along the  $z$ -axial direction on this configuration of the 3-DoF CPS. Utilizing (15) and (20) from the aforementioned conclusions, the translational displacements of each axial coordinate were separated from the 3-DoF integral compliant parallelogram mechanism.

Simultaneously, a minor difference existed between the simulation results and the theoretical calculation values. This discrepancy primarily arises from solely considering the integral deformation of the compliant guidance mechanism, but without individually incorporating the local deformation of the flexible elements in the theoretical analysis. Nevertheless, the local deformation of these flexible elements had an insignificant effect on the motion accuracy of the whole compliant mechanism from a macroscopic viewpoint.

Table 4. Analytical and FEA maximum displacement results for the 3-DoF CPS

Coordinate direction	Translational displacements (mm)	Theoretical parasitic displacements ( $\mu\text{m}$ )	FEA parasitic displacements ( $\mu\text{m}$ )	Relative error (%)
$x$ -axis	1.7576	2.89	3.07	6.22
$y$ -axis	1.7632	2.91	3.05	4.81
$z$ -axis	1.7689	2.93	3.04	3.7

Moreover, the results of the FEA analysis for the 3-DoF-compliant guidance mechanism slightly exceed those from the theoretical calculation analysis. The major reason is that the FEA analysis not only accounted for the deformation of the flexible elements but also included the deformation of other rigid components. Actually, the relatively minor elastic deformations were caused by other rigid components under the action of external driving forces.

Furthermore, the research result shows that these measures are effective in mitigating coupling errors, such as reducing the input driving force  $F$  and the length  $l$  of the compliant guide plates, increasing the thickness  $h$  of the compliant plates and selecting the flexible materials with relatively high elastic modulus  $E$ . Simultaneous utilizing a reasonable connection configuration can help diminish the negative impact of coupling errors on various coordinate axes.

The main contribution of this work is that a novel CETM is proposed according to the different connection configurations of the 3-DoF CPS. This research also provides several feasible and effective approaches to improving the motion accuracy and performances of other multi-dimensional compliant mechanisms.

## 5. Conclusions

The original contributions of this paper are summarized at the end of Section 1. The main conclusions drawn from this work are as follows:

1. Proposing the 3-DoF series CPS based on the 1-DoF compliant mechanisms.
2. Analyses of the parasitic displacement and coupling error are conducted applying the pseudo-rigid-body theory and flexible beam bending theory.
3. Establishing the CETM for the 3-DoF CPS and analysing it as corresponding to the different topological configurations.
4. Demonstrating that the configuration of the CETM is independent of the combination order of 3-DoF CPS but related to the coordinate axial vectors of each compliant mechanism.
5. Analysing the integral deformation of different configurations of the 3-DoF-compliant mechanism through FEA method analysis. The analysis result shows that the relative error of the integral deformation is small. Furthermore, the correctness of the coupling error theory model is well verified by FEA method analysis and experiment investigation.
6. The proposed methodology is not only applicable to the 3-DoF CPS but also provides theoretical foundation for parasitic displacement and coupling errors assessment in other multi-dimensional compliant mechanisms.

In the subsequent work, the physical prototype and experimental setup will be built on the 3-DoF CPS. Meanwhile, further investigations will be conducted on the coupling errors of multi-dimensional compliant mechanisms and different topological structures.

## Acknowledgements

This work was supported by a research program financed by the National Natural Science Foundation of China under Grant No. 51975448.

## References

- [1] Howell, L. L., Midha, A., & Norton, T. W. (1996). Evaluation of Equivalent Spring Stiffness for Use in a Pseudo-Rigid-Body Model of Large-Deflection Compliant Mechanisms. *Journal of Mechanical Design*, 118(1), 126–131. <https://doi.org/10.1115/1.2826843>

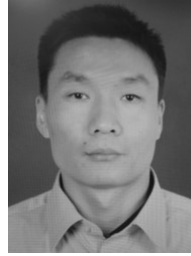
- [2] Awtar, S., Slocum, A. H., & Sevincer, E. (2006). Characteristics of Beam-Based Flexure Modules. *Journal of Mechanical Design*, 129(6), 625–639. <https://doi.org/10.1115/1.2717231>
- [3] Yin, Z., Huang, Y., Yang, H., Chen, J., Duan, Y., & Chen, W. (2022). Flexible electronics manufacturing technology and equipment. *Science China. Technological Sciences*, 65(9), 1940–1956. <https://doi.org/10.1007/s11431-022-2098-1>
- [4] Yuanqiang, L., & Wangyu, L. (2014). Analysis of the displacement of distributed compliant parallel-guiding mechanism considering parasitic rotation and deflection on the guiding plate. *Mechanism and Machine Theory*, 80, 151–165. <https://doi.org/10.1016/j.mechmachtheory.2014.06.005>
- [5] Hao, G., He, X., & Awtar, S. (2019). Design and analytical model of a compact flexure mechanism for translational motion. *Mechanism and Machine Theory*, 142, 103593. <https://doi.org/10.1016/j.mechmachtheory.2019.103593>
- [6] Li, R.-J., Fan, K.-C., Huang, Q.-X., Zhou, H., Gong, E.-M., & Xiang, M. (2016). A long-stroke 3D contact scanning probe for micro/nano coordinate measuring machine. *Precision Engineering*, 43, 220–229. <https://doi.org/10.1016/j.precisioneng.2015.08.001>
- [7] Ling, M., Yuan, L., & Zhang, X. (2024). Geometrically nonlinear analysis of compliant mechanisms using a dynamic beam constraint model (DBCM). *Mechanism and Machine Theory*, 191, 105489. <https://doi.org/10.1016/j.mechmachtheory.2023.105489>
- [8] Malaeké, H., & Moeenfarid, H. (2017). A novel flexure beam module with low stiffness loss in compliant mechanisms. *Precision Engineering*, 48, 216–233. <https://doi.org/10.1016/j.precisioneng.2016.12.004>
- [9] Awtar, S., & Mariappan, D. D. (2017). Experimental measurement of the bearing characteristics of straight-line flexure mechanisms. *Precision Engineering*, 49, 1–14. <https://doi.org/10.1016/j.precisioneng.2016.12.014>
- [10] Shi, H., Yang, G., Li, H. N., Zhao, J., Yu, H., & Zhang, C. (2024). A flexure-based and motion-decoupled XYZ nano-positioning stage with a quasi-symmetric structure. *Precision Engineering*, 89, 239–251. <https://doi.org/10.1016/j.precisioneng.2024.06.014>
- [11] Zhang, C., Yu, H., Yang, M., Chen, S., & Yang, G. (2022). Nonlinear kinetostatic modeling and analysis of a large range 3-PPR planar compliant parallel mechanism. *Precision Engineering*, 74, 264–277. <https://doi.org/10.1016/j.precisioneng.2021.09.019>
- [12] Hao, G., & Yu, J. (2016). Design, modelling and analysis of a completely-decoupled XY compliant parallel manipulator. *Mechanism and Machine Theory*, 102, 179–195. <https://doi.org/10.1016/j.mechmachtheory.2016.04.006>
- [13] Ni, Z., Zhang, D., Wu, Y., Tian, Y., & Hu, M. (2010). Analysis of parasitic motion in parallelogram compliant mechanism. *Precision Engineering*, 34(1), 133–138. <https://doi.org/10.1016/j.precisioneng.2009.05.001>
- [14] Li, J., Cai, J., Wen, J., Zhang, Y., & Wan, N. (2020). A parasitic type piezoelectric actuator with the asymmetrical trapezoid flexure mechanism. *Sensors and Actuators A: Physical*, 309, 111907. <https://doi.org/10.1016/j.sna.2020.111907>
- [15] Wu, H., Lai, L., Zhang, L., & Zhu, L. (2022). A novel compliant XY micro-positioning stage using bridge-type displacement amplifier embedded with Scott-Russell mechanism. *Precision Engineering*, 73, 284–295. <https://doi.org/10.1016/j.precisioneng.2021.09.014>
- [16] Wu, K., Zheng, G., & Hao, G. (2021). Efficient spatial compliance analysis of general initially curved beams for mechanism synthesis and optimization. *Mechanism and Machine Theory*, 162, 104343. <https://doi.org/10.1016/j.mechmachtheory.2021.104343>

- [17] Cui, L., & Awtar, S. (2019). Experimental validation of complex non-minimum phase zeros in a flexure mechanism. *Precision Engineering*, 60, 167–177. <https://doi.org/10.1016/j.precisioneng.2019.08.002>
- [18] Arredondo-Soto, M., Cuan-Urquizo, E., & Gómez-Espinosa, A. (2022). The compliance matrix method for the kinetostatic analysis of flexure-based compliant parallel mechanisms: Conventions and general force–displacement cases. *Mechanism and Machine Theory*, 168, 104583. <https://doi.org/10.1016/j.mechmachtheory.2021.104583>
- [19] Meli, F., Kueng, A., & Thalmann, R. (2005). Ultra precision micro-CMM using a low force 3D touch probe. In J. E. Decker & G.-S. Peng (Eds.), *SPIE Proceedings* (Vol. 5879, p. 58790S). SPIE. <https://doi.org/10.1117/12.618692>
- [20] Gallardo, A. G., & Pucheta, M. A. (2024). Synthesis of parallel flexure stages with decoupled actuators using sum, intersection, and difference of screw systems. *Mechanism and Machine Theory*, 192, 105526. <https://doi.org/10.1016/j.mechmachtheory.2023.105526>
- [21] Ling, M., Howell, L. L., Cao, J., & Chen, G. (2020). Kinetostatic and Dynamic Modeling of Flexure-Based Compliant Mechanisms: A Survey. *Applied Mechanics Reviews*, 72(3). <https://doi.org/10.1115/1.4045679>
- [22] Xu, H., Zhang, X., Wang, R., Zhang, H., & Liang, J. (2023). Design of an SMA-driven compliant constant-force gripper based on a modified chained pseudo-rigid-body model. *Mechanism and Machine Theory*, 187, 105371. <https://doi.org/10.1016/j.mechmachtheory.2023.105371>
- [23] Mattson, C. A., Howell, L. L., & Magleby, S. P. (2004). Development of Commercially Viable Compliant Mechanisms Using the Pseudo-Rigid-Body Model: Case Studies of Parallel Mechanisms. *Journal of Intelligent Material Systems and Structures*, 15(3), 195–202. <https://doi.org/10.1177/1045389x04033256>
- [24] Sorgonà, O., Serafino, S., Giannini, O., & Verotti, M. (2024). Analysis of compliant mechanisms with series and parallel substructures through the ellipse of elasticity theory. *International Journal of Solids and Structures*, 298, 112847. <https://doi.org/10.1016/j.ijsolstr.2024.112847>
- [25] Bai, R., Chen, G., & Awtar, S. (2021). Closed-form solution for nonlinear spatial deflections of strip flexures of large aspect ratio considering second order load-stiffening. *Mechanism and Machine Theory*, 161, 104324. <https://doi.org/10.1016/j.mechmachtheory.2021.104324>
- [26] Wang, F., Zhao, X., Huo, Z., Shi, B., Liang, C., Tian, Y., & Zhang, D. (2021). A 2-DOF nano-positioning scanner with novel compound decoupling-guiding mechanism. *Mechanism and Machine Theory*, 155, 104066. <https://doi.org/10.1016/j.mechmachtheory.2020.104066>
- [27] Li, C., & Chen, S.-C. (2023). Design of compliant mechanisms based on compliant building elements. Part I: Principles. *Precision Engineering*, 81, 207–220. <https://doi.org/10.1016/j.precisioneng.2023.01.006>
- [28] Ochoa, O., Betancourt-Tovar, M., Espinosa-Curiel, A. S., Castro-Avilés, A., Granados, N., & Cuan-Urquizo, E. (2024). Novel compliant mechanism-based auxetic metamaterial: Kinematic and experimental analysis. *International Journal of Mechanical Sciences*, 279, 109478. <https://doi.org/10.1016/j.ijmecsci.2024.109478>





**Huaibo Qiang** received the M.Sc. degree in engineering from Xi'an Technological University, China, in 2007. As a lecturer, he has been engaged in teaching and research work on mechanical and electrical engineering for over twenty years. His research focuses on precision measurement theory and instrument design, compliant mechanism design theory and application. He is currently pursuing a Ph.D. degree in Mechanical and Electronic Engineering.



**Qiang Huang** received the M.Sc. degree in engineering from Xi'an Technological University, China, in 2007. He is currently a senior engineer at the Northwest Institute of Mechanical and Electrical Engineering. His research activities focus on the analysis of complex structural forces and the integration of electromechanical systems.



**Hongxi Wang** received the Ph.D., degree from Xidian University, China, in 2006. He is currently a Full Professor and the Dean of School of Mechatronic Engineering in Xi'an Technological University. His research activity focuses on precision measurement theory and instrument design, compliant mechanisms and intelligent sensors.